Enceladus: An Active Ice World in the Saturn System

John R. Spencer[1] and Francis Nimmo[2]

[1]Department of Space Studies, Southwest Research Institute, Boulder, Colorado 80302; email: spencer@boulder.swri.edu

[2]Department of Earth and Planetary Sciences, University of California, Santa Cruz, California 95064; email: fnimmo@es.ucsc.edu

Annu. Rev. Earth Planet. Sci. 2013. 41:693–717

The *Annual Review of Earth and Planetary Sciences* is online at earth.annualreviews.org

This article's doi:
10.1146/annurev-earth-050212-124025

Keywords

tidal heating, planetary satellites, cryovolcanism, habitability, tectonics

Abstract

Enceladus, one of the mid-sized icy moons of Saturn, has an importance to planetary science far greater than its modest 504-km diameter would suggest. Intensive exploration of Enceladus by the Cassini Saturn orbiter has revealed that it is the only known icy world in the solar system with ongoing deep-seated geological activity. Active tectonic fractures at Enceladus's south pole, dubbed "tiger stripes," warmed by internal tidally generated heat, spew supersonic jets of water vapor, other gases, and ice particles into circum-Saturnian space. A subsurface saltwater sea probably exists under the south pole, between the ice shell and the silicate core. Because of evidence that liquid water is probably present at the jet sources, Enceladus is also of great astrobiological interest as a potential habitat for life.

1. INTRODUCTION

Enceladus (**Figure 1**) is one of five mid-sized satellites, Mimas, Enceladus, Tethys, Dione, and Rhea (in order of increasing distance from the planet), ranging from 400 to 1,500 km in diameter (**Figure 2**), orbiting Saturn beyond the main ring system and associated small satellites, and interior to the giant moon Titan. All these moons are large enough to be spherical or nearly so, and all are relatively low density, high albedo bodies with water ice/silicate interiors and surfaces composed mainly of water ice. With the notable exception of Enceladus, all have surfaces that are dominated by impact craters, leading researchers to infer that they have been largely inactive for billions of years.

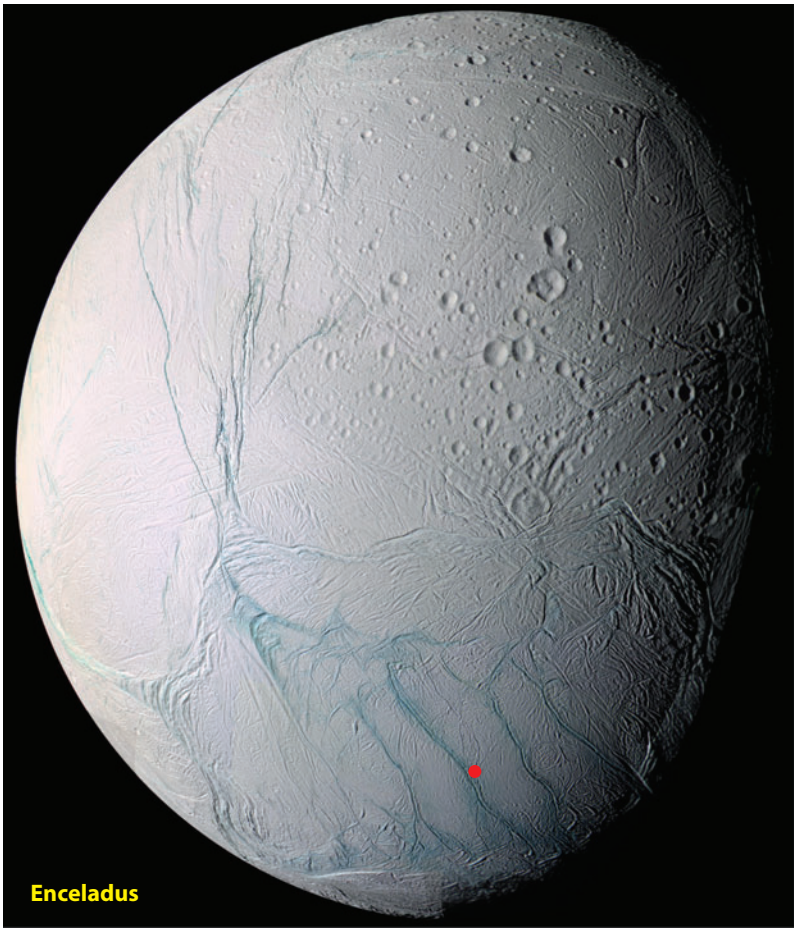

Figure 1

Global view of Enceladus (diameter 504 km) obtained by the Cassini cameras on July 14, 2005, centered approximately at longitude 195°W, latitude 40°S. Older cratered terrain is visible in the upper right, and tectonically disrupted terrain of intermediate age is visible in the upper left. The active south polar terrain occupies the lower part of the image: The red dot indicates the south pole. The four parallel bluish fractures surrounding the south pole are the tiger stripes, which are the source of Enceladus's plumes. The tiger stripes, and some other fractures, appear blue because they are rich in coarse-grained water ice, which absorbs the near-infrared light used to create the red channel in this false-color image. NASA image release PIA0625 (NASA/JPL/Space Science Institute).

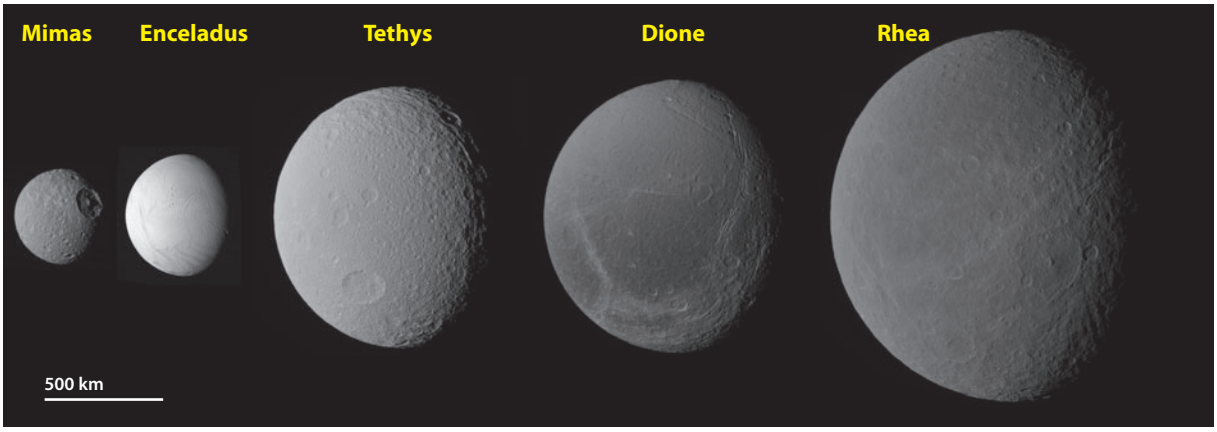

Figure 2

The five inner mid-sized satellites of Saturn, shown to scale with comparable lighting and approximately correct relative brightness. Enceladus is distinguished by its high albedo and relatively youthful, uncratered surface. Composite of Cassini images by E. Lakdawalla.

Owing to mutual gravitational interactions, Enceladus is locked in a 2:1 eccentricity-type orbital resonance with the larger moon Dione, orbiting Saturn twice for every orbit of Dione. As described in Section 3 (see below), this resonance plays a key role in maintaining Enceladus's unusual geological activity via tidal heating. Similarly, Mimas orbits in a 2:1 inclination-type resonance with Tethys. In the early 1980s, ground-based observations revealed Enceladus's spatial association with Saturn's tenuous outer "E" ring, and the *Voyager* Saturn flybys discovered its complex and youthful surface geology and extremely high albedo (Smith et al. 1982). On the basis of these discoveries, some suggested that ongoing geyser-like activity on Enceladus may be creating the E-ring (Haff et al. 1983), but proof was lacking and other possibilities were also considered (e.g., Hamilton & Burns 1994). The NASA/ESA Cassini Saturn orbiter provided necessary proof within little more than a year of arrival at Saturn, culminating in a close flyby in July 2005, complemented by distant imaging observations, which discovered the south polar particle and gas plumes as well as the complex geological province termed the south polar terrain (SPT) with its warm "tiger stripe" fractures, which are the source of the plumes. The discovery made Enceladus a high priority target for future Cassini exploration, and the spacecraft has now completed 20 close flybys at altitudes between 20 and 5,000 km, including many passages directly through the plume.

Thanks to Cassini's superb and diverse instrumentation, these flybys have yielded a wealth of information about Enceladus and its activity, as described in the first part of this review. We then discuss how analysis of these data has given us the beginnings of an understanding of how Enceladus works, providing a primer for understanding former activity on other icy worlds and providing intriguing hints that habitable environments may exist in its interior. We focus on Enceladus but do not do justice to its fascinating interaction with the Saturnian magnetosphere. For a more extensive review of earlier work, see Spencer et al. (2009).

2. OBSERVATIONS

2.1. Density, Gravity, Shape

The bulk density of Enceladus is $1{,}609 \pm 5$ kg m^{-3} (Thomas 2010), suggesting a roughly 60:40 rock:ice mixture by mass (Schubert et al. 2007). Unfortunately, observational constraints on the

polar moment of inertia C are lacking. Its global shape is unexpected for a hydrostatic body (see below), preventing application of the Darwin-Radau approximation (Murray & Dermott 1999), and gravity measurements (Ducci et al. 2012) are currently too preliminary to interpret, though new data obtained in spring 2012 may provide more definitive results. Giese et al. (2011) have argued that Enceladus exhibits rotational librations forced by Dione. These are difficult measurements to make, but if correct, they suggest some degree of mass concentration toward the center. The amplitude of the librations is too small to induce significant tidal heating from libration alone (cf. Wisdom 2004). Enceladus's obliquity, which is potentially diagnostic of its moment of inertia, is expected to be ~0.001° (Chen & Nimmo 2011), too small to measure.

Satellites without rigidity will adopt a hydrostatic shape. All three inner moons—Mimas, Enceladus, and Tethys—have shapes that are nonhydrostatic (Thomas 2010), due to elastic, dynamic (e.g., convection), or isostatic processes (Section 3.2). At 100-km-scale wavelengths, the topography is notably bumpy: Ovoid depressions and bulges ~1 km in amplitude are present (Schenk & McKinnon 2009, Nimmo et al. 2011) (**Figure 3**). The depressions in general do not correlate with surface features, with the notable exception of a 0.7-km-deep depression at the south pole. In contrast, Enceladus is anomalously smooth at ~10-km wavelengths (Nimmo et al. 2011), perhaps as a result of relaxation.

2.2. Global Geology

Enceladus's surface geology is extremely diverse and is strangely symmetrical (Crow-Willard & Pappalardo 2010; E.N. Crow-Willard & R.T. Pappalardo, submitted) (**Figure 4**) about both its rotation axis and the direction of Saturn (which is fixed relative to Enceladus's surface, as a result of its synchronous rotation). Absolute ages of surfaces can be estimated from the density

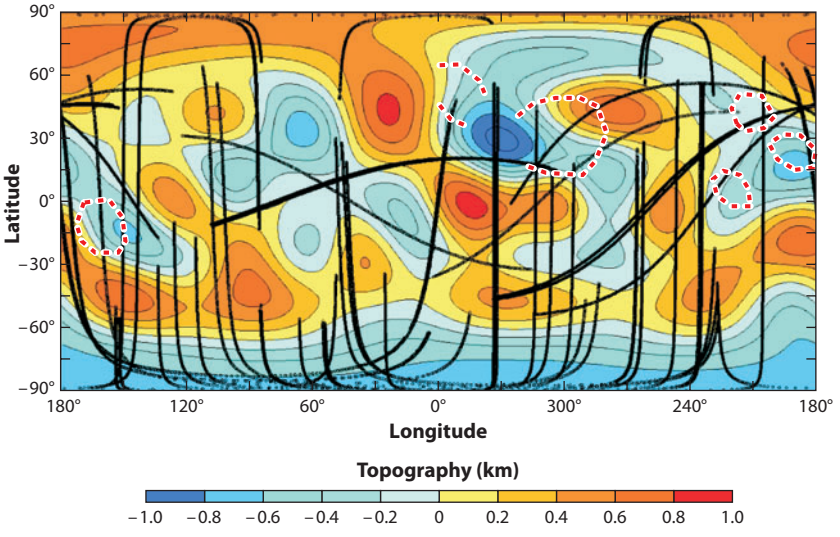

Figure 3

Long-wavelength topographic map of Enceladus. Red dashed lines indicate topographic depressions identified by Schenk & McKinnon (2009), and black lines are limb profile traces used to derive topography. From Nimmo et al. (2011). Copyright 2012 American Geophysical Union. Adapted with permission from the American Geophysical Union.

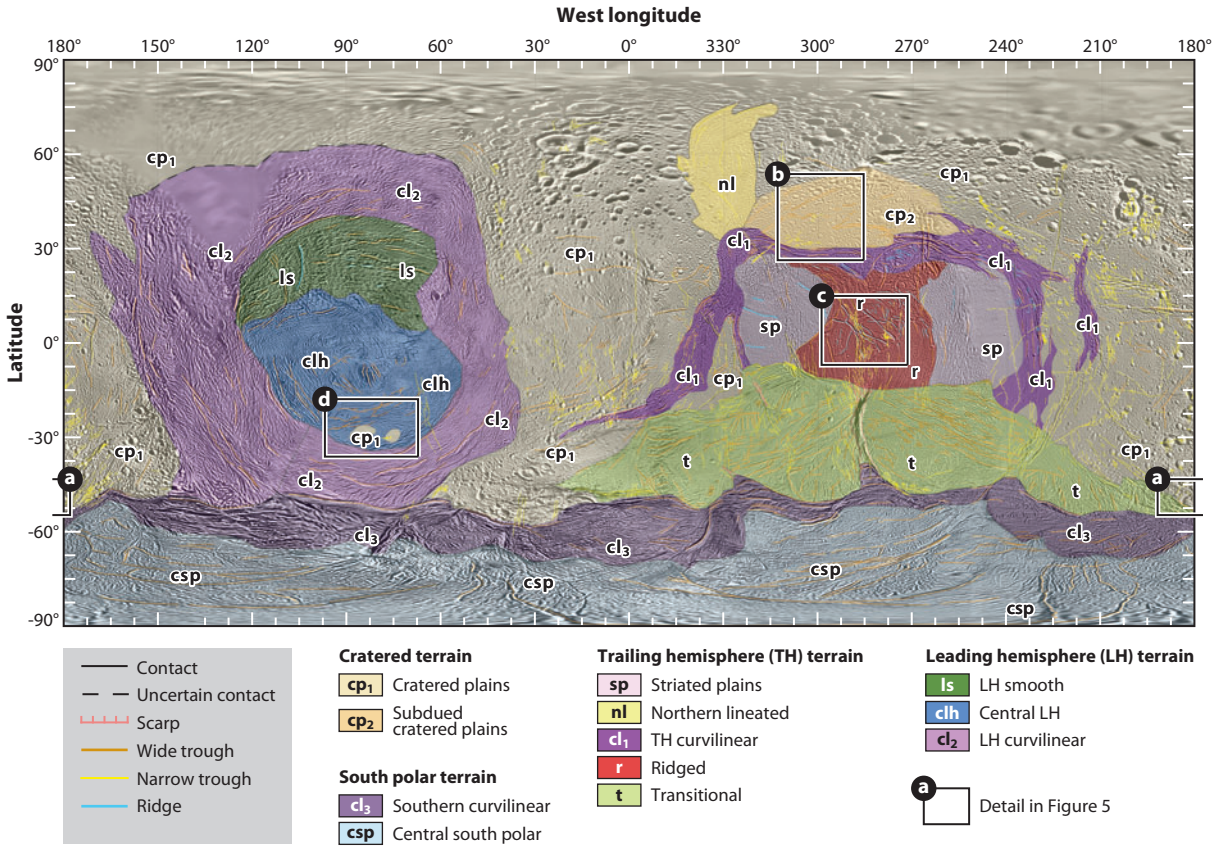

Figure 4

Geological map of Enceladus (Crow-Willard & Pappalardo 2011; E.N. Crow-Willard & R.T. Pappalardo, submitted). Longitude is defined so the Saturn-facing, leading, anti-Saturn, and trailing hemispheres are approximately centered at longitudes 0°W, 90°W, 180°W, and 270°W, respectively. The labeled rectangles show the locations of the images in **Figure 5**. Copyright 2013 American Geophysical Union. Adapted with permission from the American Geophysical Union.

of superposed impact craters and models of the impactor flux, but they are uncertain to within a factor of two or more (Dones et al. 2009, Kirchoff & Schenk 2009).

The oldest terrains on Enceladus are cratered regions (**Figure 5*a***) forming a continuous band extending from the Saturn-facing side, over the north pole, to the anti-Saturn side (**Figure 4**), with surface ages in the 1–4-Ga range (Kirchoff & Schenk 2009). However, most craters have been heavily modified since their formation by pervasive tectonic fracturing and by a combination of viscous relaxation and burial (perhaps by ejecta from plumes), as a result of which many craters are unusually shallow (Bland et al. 2012) (**Figure 5*a*,*b***).

Centered on the leading and trailing hemispheres of Enceladus are younger provinces (**Figure 4**), with ages from 2 Ga to 10 Ma, which are dominated by intense tectonism (**Figure 5*c*,*d***), including crosscutting curved sets of parallel ridges and grooves with amplitudes of ~1 km (Giese et al. 2008), large regions of aligned small hills, and isolated ridges and fractures. The appearance of the fractures and ridges suggests extensive, nonrigid, lateral motion, involving both extensional and compressional stresses. Structures in each province are quite symmetrical about the apex and antapex of motion (Crow-Willard & Pappalardo 2011), and on the trailing

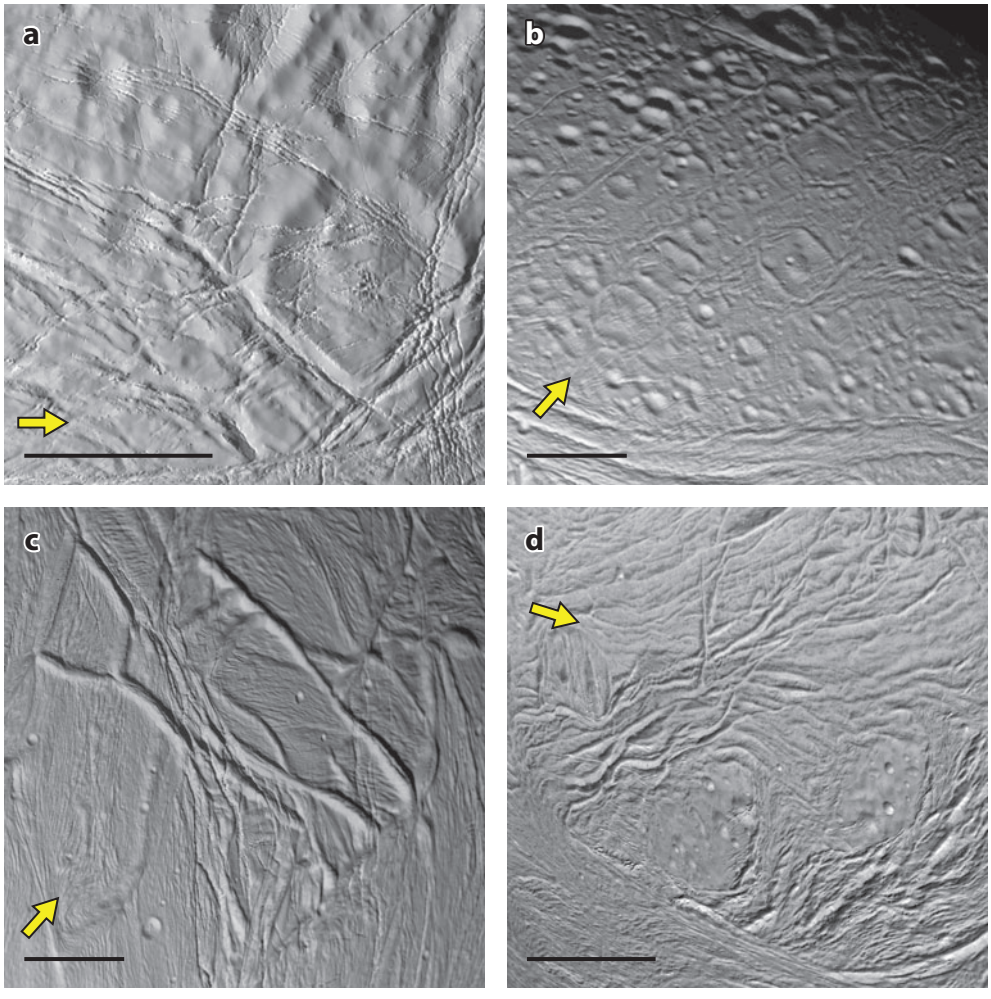

Figure 5

Examples of Enceladus terrain types (Crow-Willard & Pappalardo 2011; E.N. Crow-Willard & R.T. Pappalardo, submitted) (see **Figure 4**). (*a*) Craters at the edge of the heavily cratered terrain, perhaps mantled by plume fallout, showing the pervasive fracturing of the cratered terrain. (*b*) Subdued cratered plains in which craters have apparently been flattened by viscous relaxation of the crust. (*c*) Ridged terrain, perhaps produced by compression, in the trailing hemisphere. Scattered impact craters show that this terrain is older than the crater-free active south polar terrain (**Figure 6**). (*d*) Islands of heavily cratered terrain, surrounded by intensely deformed leading hemisphere terrains. The scale bar is 20 km long in all images, and the yellow arrow shows the direction of solar illumination. See **Figure 4** for image locations.

hemisphere, crater densities, and therefore ages, decrease from north to south (Kirchoff & Schenk 2009). These provinces include many topographic features that are similar to those in the active south polar region (Spencer et al. 2009), but they lack obvious analogs to the tiger stripe fractures where south polar activity is currently focused.

Small-scale topographic features have been used to infer ancient heat fluxes. Giese et al. (2008) used a flexural analysis of equatorial rifts to derive an elastic thickness of 0.3 km and a heat flux (neglecting porosity) of 200–270 mW m^{-2}. Bland et al. (2007) analyzed equatorial ridges and troughs to obtain an elastic thickness of 0.4–1.4 km and a heat flux of 110–220 mW m^{-2}. Some

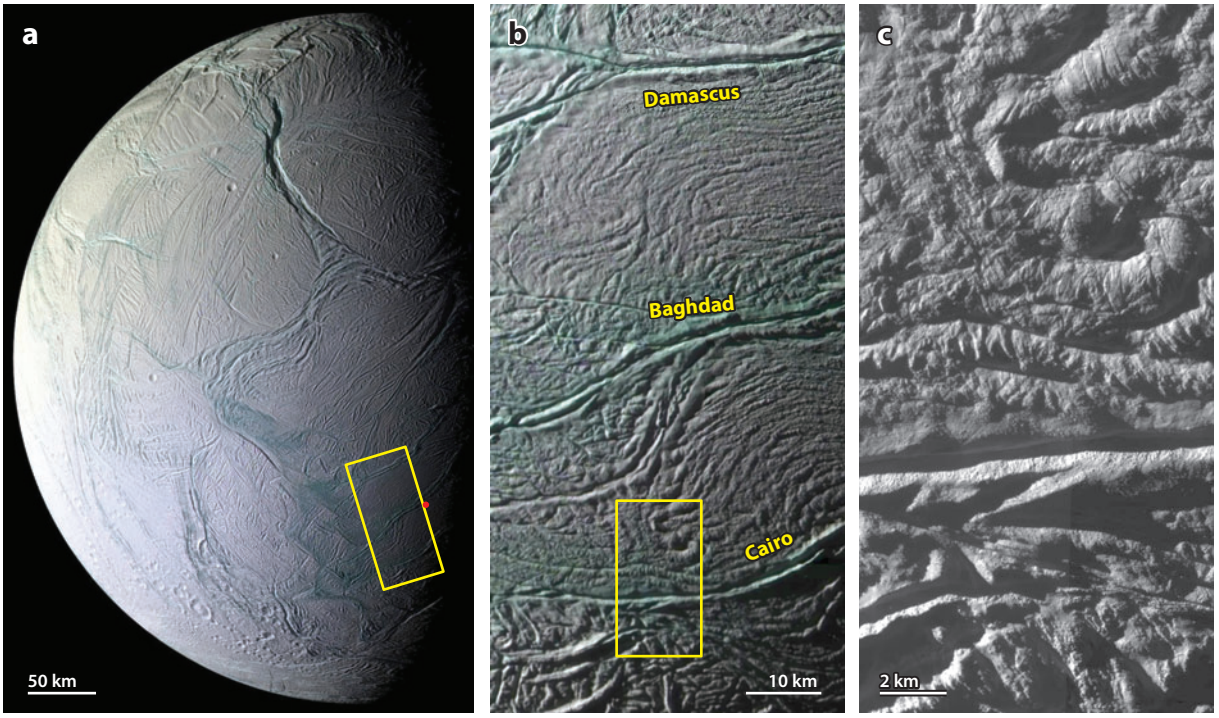

Figure 6

Cassini images of the south pole of Enceladus at a variety of scales, taken in late 2008. (*a*) Global view, centered approximately at longitude 285°W, latitude 65°S. A red dot marks the south pole, and the yellow rectangle marks the location of panel *b*. (*b*) The prominent fractures are the tiger stripes Damascus Sulcus, Baghdad Sulcus, and Cairo Sulcus, and the yellow rectangle marks the location of panel *c*. (*c*) Close-up of part of Cairo Sulcus and surrounding terrain. One of the plume jets identified by Spitale & Porco (2007) erupts from this portion of Cairo Sulcus. From NASA image releases PIA11133, PIA11112, and PIA11114 (NASA/JPL/Space Science Institute).

relaxed craters (**Figure 4*b***) suggest heat fluxes in excess of 150 mW m^{-2} (Bland et al. 2012). These heat flux estimates are comparable to the present-day output of the south polar region (Section 2.3) and suggest comparable levels of geological activity when, or at some time after, these features formed.

2.3. The Active South Polar Terrain

Continuing the pattern of global symmetry, present-day geological activity on Enceladus appears to be centered almost precisely on the south pole, at the center of a distinct geological province called the South Polar Terrain (SPT) (Porco et al. 2006). The SPT is bounded by south-facing scarps and rugged marginal arcs (ridge belts) at around latitude 50°S (**Figures 1**, **4**, and **6*a***). Southward of this boundary, the pervasively fractured surface has almost no impact craters, suggesting a surface age of less than a few million years (Porco et al. 2006). In three places where the boundary bulges northward on the trailing hemisphere, young sets of extensional fractures extend northward into the older terrains. The four tiger stripes are located in the center of the SPT where most current activity appears to be concentrated (**Figures 1**, **6**, and **7**). These are prominent parallel fractures, approximately 130 km long and spaced 35 km apart, striking approximately 30° from

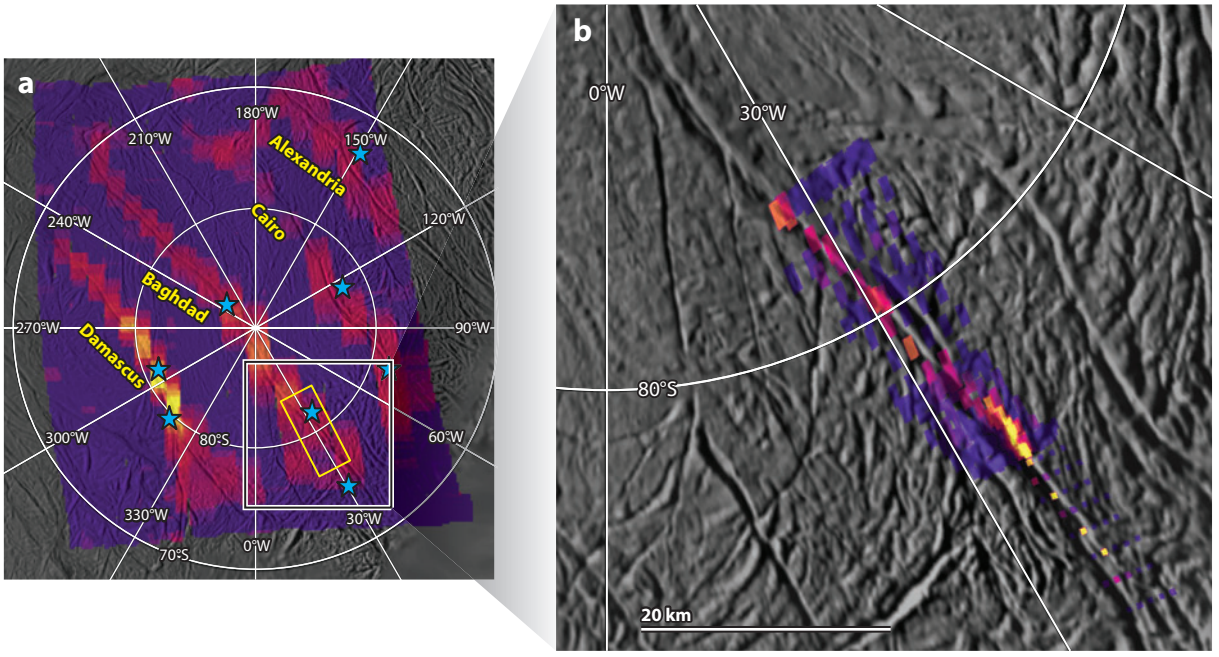

Figure 7

Thermal emission at 10–17 μm from the tiger stripes as mapped by Cassini, superposed on a map based on visible-wavelength images. Purple indicates negligible thermal emission, and warmer colors indicate increasing intensity of emission. (*a*) Almost the entire tiger stripe system, observed on March 12, 2008. The blocky appearance is due to the relatively low spatial resolution (4–10 km) of the infrared instrument in this observation. Blue stars show the inferred location of plume jets (Spitale & Porco 2007). (*b*) A higher spatial resolution (~1 km) observation of the thermal emission from part of Baghdad Sulcus taken on November 21, 2009, showing the narrow confinement of the emission to the tiger stripe fracture. From NASA image release PIA12448 (NASA/JPL/GSFC/SwRI/Space Science Institute).

the direction to Saturn. The tiger stripe fractures have raised margins enclosing a central trough approximately 2 km wide and 0.5 km deep (**Figure 6*c***), which is the source of both thermal emission (Spencer et al. 2006, 2009) (**Figure 7**) and the plume jets (Spitale & Porco 2007, Porco et al. 2013) (**Figure 8**). Measurements of the thermal emission show that surface temperatures within the troughs reach at least 180 K over regions tens of meters wide along the length of the tiger stripes (Spencer et al. 2009, 2011). The current best estimate of the total endogenic power radiated by the tiger stripes and their surroundings, based on direct measurements of the infrared emission by Cassini, is 15.8 ± 3.1 GW (Howett et al. 2011). However, this is a difficult measurement, because of the need to estimate and subtract the portion of the thermal radiation due to absorbed solar radiation. Thus, the true uncertainty in the heat flow may be larger than the quoted errors would suggest.

2.4. Plume Structure and Composition

Multiple jets of vapor and particles erupt from the tiger stripes found on Enceladus (Spitale & Porco 2007) (**Figure 8**). These then combine at altitude to form a merged plume. The gas plume is dominated by water vapor, plus approximately 5% CO_2, 1% CH_4, 1% NH_3, and small quantities of many heavier hydrocarbons and organic molecules (Hansen et al. 2011; Waite et al. 2009,

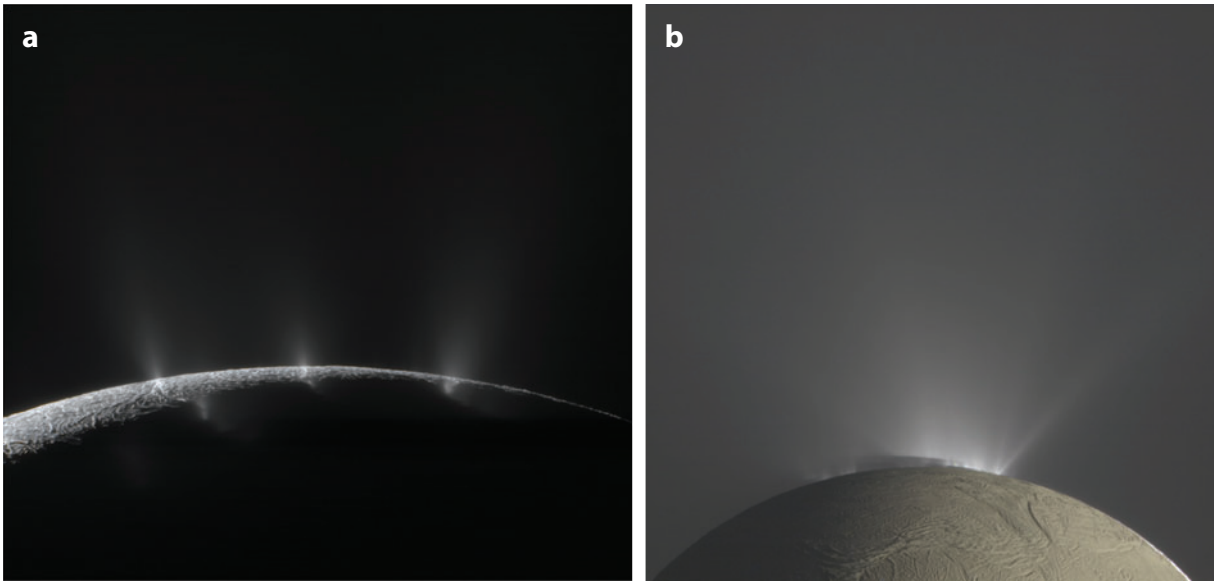

Figure 8

The particle plume jets of Enceladus, seen by the Cassini cameras. The jets are prominent here because the images are taken in forward-scattered light, looking toward the Sun, and the micrometer-sized plume particles scatter efficiently in this geometry. (*a*) Image taken on August 13, 2010, showing jets from the tiger stripes (*from left to right*) Cairo, Baghdad, and Damascus, rising into sunlight. (*b*) Image taken on November 30, 2010, with part of the night side of Enceladus illuminated by Saturn shine, though the plume jets are illuminated by direct sunlight. The lower parts of many plume jets are hidden by Enceladus's shadow or by the body of Enceladus. (NASA/JPL/Space Science Institute/Gordan Ugarkovic.)

2011). The plume particles are predominantly water ice, but most contain approximately 1% salt, mostly NaCl (Postberg et al. 2011), and have typical radii of a few micrometers. Ingersoll & Ewald (2011) estimate that half the mass is in particles with radii greater than 3 μm. The speed of the ejected material can be estimated from its vertical distribution and the collimation of the jets. The particles appear to have a wide range of speeds, with ∼10% exceeding the escape speed of 240 m s^{-1} (Ingersoll & Ewald 2011). The gas speed is harder to constrain but appears to be faster than that of most of the dust particles (Schmidt et al. 2008). The current best estimate is ∼450 m s^{-1}, with some jets perhaps reaching 1 km s^{-1} (Hansen et al. 2011). Estimated vent production rates from Enceladus are ∼200 kg s^{-1} for the gas (Hansen et al. 2011) and up to ∼50 kg s^{-1} for the dust (Ingersoll & Ewald 2011). However, it is likely that most of the gas escapes Enceladus, whereas only ∼10% of the dust escapes, because most dust grains, particularly the larger and more salt-rich ones (Hedman et al. 2009, Postberg et al. 2011) do not reach escape speed. There are preliminary indications of a possible correlation of the plume's near-infrared brightness with Enceladus's position in its orbit, suggesting modulation of plume activity by diurnal tidal flexing (Gosmeyer et al. 2013).

2.5. Surface Structure and Composition

Enceladus has the highest albedo of any known solar system object, reflecting ∼80% of the sunlight that it intercepts (Howett et al. 2010). This is undoubtedly due to a surface coating of reimpacted ice-rich plume particles (Kempf et al. 2010), a conclusion strengthened by the remarkable

agreement between the predicted spatial distribution of plume fallout (Kempf et al. 2010) and subtle surface color patterns seen by Cassini's cameras (Schenk et al. 2011). Not surprisingly, the surface composition, as determined by near-infrared spectroscopy, is almost pure water ice (Newman et al. 2008). Inferred ice-grain size varies across the surface: The largest sizes are found near the tiger stripes, as revealed by infrared spectroscopy (Jaumann et al. 2008) and 1-μm imaging (Porco et al. 2006). Spectroscopic evidence also indicates small amounts of CO_2 (Brown et al. 2006), H_2O_2 or light organics (Brown et al. 2006, Newman et al. 2007), and perhaps NH_3 (Emery et al. 2005). Apart from H_2O_2, which could be produced by surface oxidation of H_2O, surface composition is consistent with the observed plume composition. The salts seen in the plume particles have bland reflectance spectra and thus cannot be detected on Enceladus's surface. Surface temperatures at low latitudes vary from ~50 K at night to ~80 K during the day (Howett et al. 2010). The diurnal temperature variation implies a very low surface thermal conductivity and a fluffy unconsolidated surface, as expected for plume particle fallout, though surface thermal conductivity is not dramatically lower than that of other icy Saturnian satellites.

2.6. Influence on the Saturn System

It is now well established that the E ring, which first drew attention to Enceladus in the 1980s, is generated by particles from Enceladus's south polar plume (Kempf et al. 2010) (**Figure 9**). Although comprising ~6% salt-rich particles (Postberg et al. 2009), the E ring consists

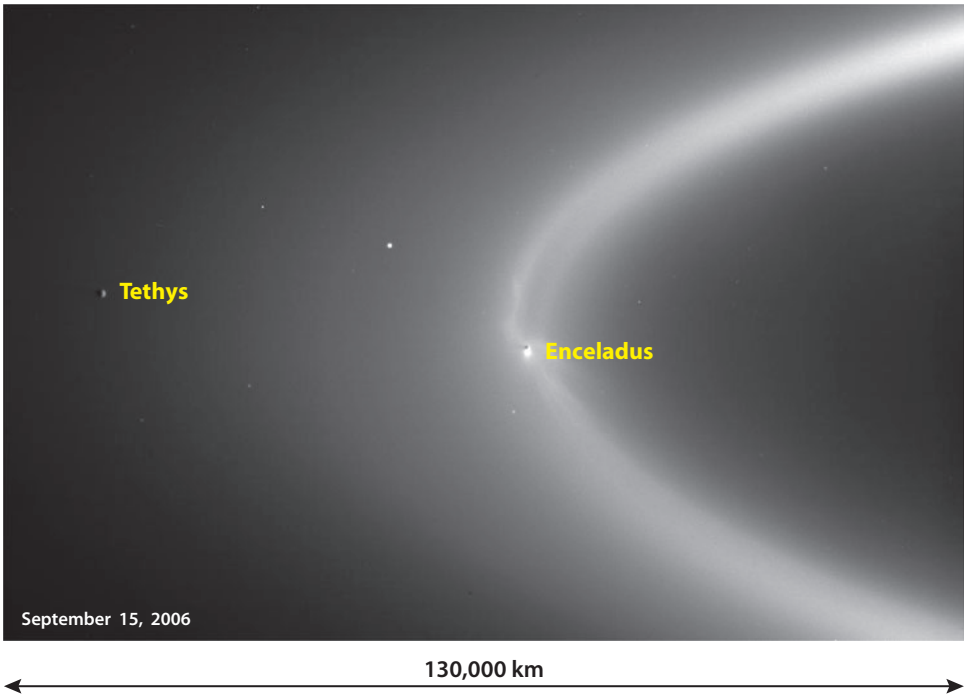

Figure 9

Enceladus (*black dot*, *center*) and Saturn's E ring, seen in forward-scattered light on September 15, 2006, showing the intimate relationship between Enceladus and the ring. The bright dot on the far left is the moon Tethys, which in contrast has no associated ring. Other bright points are background stars. From NASA image release PIA08321 (NASA/JPL/Space Science Institute).

preferentially of the smaller, salt-poor plume particles, which have the highest speeds and, thus, most readily escape Enceladus. Saturn's other mid-sized satellites decrease in brightness with distance from Enceladus, suggesting that impacts by E-ring particles have a large effect on their surfaces (Verbiscer et al. 2007). Most of the E-ring particles are destroyed by sputtering on timescales of decades (Juhasz & Horanyi 2002, Ingersoll & Ewald 2011). Harder to detect is Enceladus's torus of neutral OH, H_2O, and O (Esposito et al. 2005, Hartogh et al. 2011, Shemansky et al. 1993), derived from the water vapor in the Enceladus plume (Johnson et al. 2006). Despite the presence of some NaCl-rich particles in the E ring, atomic sodium is not detected in the E-ring region (Schneider et al. 2009). Thanks to Enceladus's prodigious output, neutral species are much more important in Saturn's magnetosphere than in Jupiter's magnetosphere (Mauk et al. 2009). Water from Enceladus may even be a major source of oxygen in the atmospheres of Titan and Saturn (Cassidy & Johnson 2010). Enceladus's interaction with the Saturnian magnetosphere is complex: Negatively charged dust plays a surprising important role (Morooka et al. 2011). The interaction drives electrical currents along magnetic field lines, thereby producing a "footprint" of ultraviolet auroral emission near Saturn's poles (Pryor et al. 2011).

3. UNDERSTANDING: ORIGIN AND INTERIOR

3.1. Bulk Structure

Figure 10 shows our interpretation of Enceladus's interior. Given the high observed heat output, Enceladus is almost certainly a fully differentiated body, though definitive evidence is not yet in hand. Based on the observed bulk density, the radius of the metal-silicate core is then roughly 150–170 km, overlain by an ice/water layer 80–100 km thick (Schubert et al. 2007). The detection of Na in the erupted ice particles (Postberg et al. 2011) is most readily explained by the presence of liquid water that at some point was in contact with silicates (Zolotov 2007).

In the silicate core, heating by tides (see Section 3.3) is expected to be negligible owing to the high silicate rigidity and viscosity (Roberts & Nimmo 2008a). Present-day radiogenic heating within the core is expected to generate approximately 0.3 GW. Tidal heating within the ice shell can be much larger, especially if it is at least locally decoupled from the underlying silicates by liquid water.

The presence of the pronounced south polar depression can be readily explained by a subsurface, regional "sea" (Collins & Goodman 2007). As discussed in Section 3.5, maintaining a global ocean over geological time is very difficult. Ammonia is an efficient antifreeze (Hogenboom et al. 1997) and has been detected in the plumes at ~1% concentration (Waite et al. 2009). Higher concentrations of NH_3 in the ocean could delay (but not prevent) complete freezing of a global ocean. Conversely, if tidal heating and liquid water are both confined to the south polar region, then steady-state situations permitting a regional sea and matching the observed heat output can be constructed (e.g., Tobie et al. 2008).

3.2. Ice Shell Convection and Density Variations

It is unclear whether Enceladus's ice shell can convect. The low gravity and relatively thin ice shell make convection marginal and highly dependent on uncertain parameters such as grain size (Barr & McKinnon 2007). Sustained global convection in Enceladus would make it too dissipative to be consistent with long-term orbital constraints (Zhang & Nimmo 2009) (Section 3.4). The high heat fluxes and young inferred age at the south pole could potentially be explained by localized solid-state convection, especially if the near-surface ice is weak (Barr 2008, Han et al. 2012,

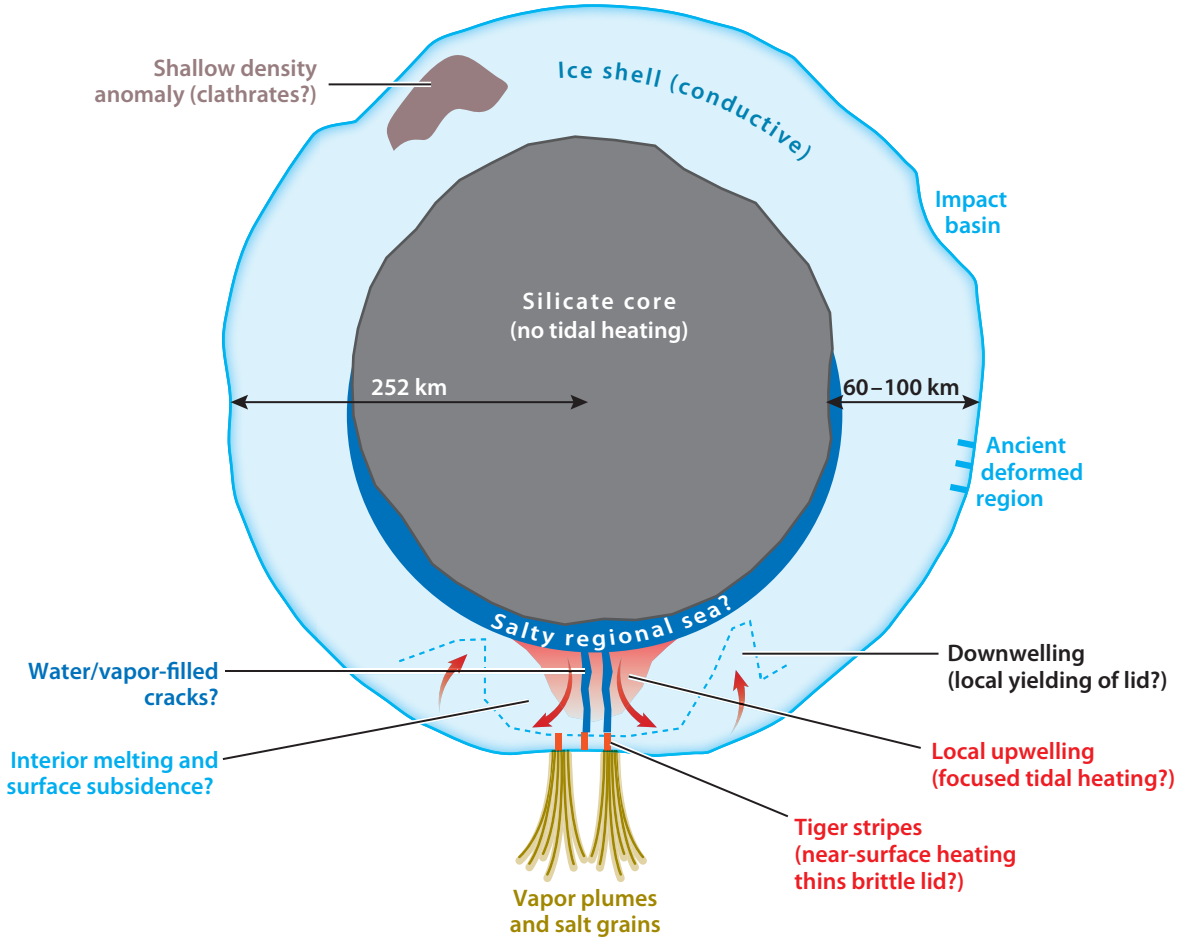

Figure 10

Diagram of Enceladus's possible interior structure. Except for the convecting, tidally heated south polar region, the ice shell is conductive, with bumpy surface topography arising from lateral density contrasts (perhaps induced by earlier tidal heating episodes). A regional sea exists beneath the south pole, maintained by tidal dissipation in the ice shell above. Salty water and heat are advected from the base of the ice shell (~100 km deep) to the jets at the surface, with additional dissipation occurring in the near surface by shear heating. The silicate core is cold, rigid, and probably irregularly shaped.

O'Neill & Nimmo 2010). However, heat transport may instead be confined to the tiger stripes and occur via conduction (in the near surface) and advection (of either liquid water or vapor) at greater depths (see Section 4.2).

The observed 1-km amplitude of global long-wavelength topography (Schenk & McKinnon 2009) (**Figure 3**) is much larger than that expected from thermal convection alone (e.g., Roberts & Nimmo 2008b). Either lateral shell thickness variations or lateral density variations could be responsible. In our view, density anomalies [which can reside at shallow depths and persist indefinitely (J. Besserer, F. Nimmo, J.H. Roberts & R.T. Pappalardo, submitted)] present a more likely explanation for most of the observed topography than do shell thickness variations, because viscous flow will rapidly remove shell thickness variations, even for conductive shells (Stevenson 2000).

The existence of ice shell lateral density variations has also been invoked to explain the polar location of the hot spot (Nimmo & Pappalardo 2006). In this picture, a region of low density is produced, for example, by convection-induced melting and drainage (e.g., Behounkova et al. 2012, Sotin et al. 2002) or by destabilization of denser clathrates (e.g., Kieffer et al. 2006). This active region then reorients to its rotationally stable location at the pole. An argument against this hypothesis, however, is the symmetry of older geological terrains about the current spin axis and Saturn direction.

3.3. Heat Source

Given the absence of other plausible mechanisms, the dominant power source for Enceladus is almost certainly tidal heating, driven by rhythmic distortions of the moon by Saturn's tides as Enceladus follows its eccentric orbit. However, most details, including the magnitude and time history of the heat source as well as the location and nature of the dissipation, are still not clear. By understanding tidal heating on Enceladus, where its effects are ongoing and obvious, we hope for a better understanding of this fundamental planetary process on other worlds as well.

Tidal heating arises when an object is in a noncircular orbit, because some of the mechanical work associated with the changing size of the tidal bulge is converted to heat. Heating in the ocean has been suggested (Tyler 2011) but requires obliquities that are unrealistically large (Chen & Nimmo 2011). Tidal dissipation in the solid shell may be broadly distributed (e.g., Behounkova et al. 2010), or it could arise from frictional heating on individual fault segments (Nimmo et al. 2007), or both. The heat radiated by the tiger stripes (**Figure 7**) could be generated there or advected from greater depths. In any event, the high observed heat production suggests the existence of at least a regional sea (Nimmo et al. 2007, Tobie et al. 2008), because an ice shell coupled directly to the silicate core underneath will not deform significantly and deformation is required to generate tidal heat.

Another mystery is why only one location on Enceladus is active. Tidal dissipation can become localized via a feedback mechanism in which a warmer (and thus more deformable) region suffers enhanced heating (e.g., Mitri & Showman 2008). Thus, it is potentially self-sustaining, although an initial perturbation of some kind is still needed (perhaps an impact?). Alternatively, the geometry of the underlying core may have favored continued polar geological activity (McKinnon 2011).

3.4. Tidal Heating and Orbital Evolution

One of the most puzzling aspects of Enceladus is the magnitude of its current heat output (approximately 16 GW). The rate of tidal heat production for a synchronous body is generally calculated as follows (e.g., Murray & Dermott 1999):

$$\dot{E} = \frac{21}{2}\frac{n^5 R^5}{G}\frac{k_2}{Q}e^2 = 15\,\mathrm{GW}\left(\frac{k_2/Q}{0.01}\right)\left(\frac{e}{0.0047}\right)^2. \quad (1)$$

Here n is the mean orbital motion (5.3×10^{-5} s^{-1}); R is the satellite radius (252 km); G is the gravitational constant; e is the satellite eccentricity (0.0047); k_2 is the tidal Love number, which describes the amplitude of the diurnal tidal flexing; and Q is the dimensionless dissipation factor. Highly deformable and dissipative bodies have large k_2/Q values.

Tidal heating depends mainly on the body's orbital eccentricity and k_2/Q. For an isolated satellite, dissipation rapidly damps the orbital eccentricity. However, an orbital resonance with another satellite can act to increase eccentricity and thus maintain the dissipation. In Enceladus's

case, its present-day eccentricity, and thus its dissipation, is maintained by a 2:1 eccentricity-type mean motion resonance with Dione (Meyer & Wisdom 2008a).

In the particular case that Enceladus's eccentricity remains constant, the heat production within Enceladus is inversely proportional to Saturn's Q and is independent of Enceladus's k_2/Q (Meyer & Wisdom 2007). In this case, the eccentricity adjusts itself to produce the equilibrium heating rate (Equation 1), depending on the value of Enceladus's k_2/Q.

The time-averaged Q of Saturn is generally assumed to exceed 18,000—if it were smaller, Mimas would have been inside Saturn's Roche limit later than 4.5 Ga B.P. (Meyer & Wisdom 2007). If $Q_{\text{Saturn}} > 18{,}000$, then the upper bound on the time-averaged heat production within Enceladus is 1.1 GW (Meyer & Wisdom 2007). This is an order of magnitude smaller than the currently observed heat flow. How can this apparent paradox be resolved? There are four main possibilities.

First, perhaps the current Q of Saturn is much smaller than 18,000, as suggested by a recent interpretation of astrometric data (Lainey et al. 2012). We cannot rule out this hypothesis but do not favor it, mainly because the astrometric analysis also shows rapid inward motion of Mimas, which is difficult to explain. A smaller Saturn Q is also difficult to reconcile with the current locations of the satellites unless the mid-sized satellites are significantly younger than the solar system (cf. Charnoz et al. 2011).

Second, perhaps Enceladus is producing heat at the appropriate time-averaged rate (1.1 GW), but this heat is released episodically. This may be plausible for convecting ice on Enceladus (O'Neill & Nimmo 2010). **Figure 11** shows the variation of surface heat flux with time for one such model, demonstrating that peak heat fluxes of order 200 mW m^{-2} can be obtained, with a periodicity of order 100 Ma and a duty cycle of a few percent. Episodic heat release may also be compatible with a situation in which the heat is advected from a subsurface ocean via water-filled cracks (see below).

Third, and perhaps most likely, Enceladus may be manifesting episodic heat production (e.g., Ojakangas & Stevenson 1986; but cf. Meyer & Wisdom 2008b). In this picture, it spends ~10% of

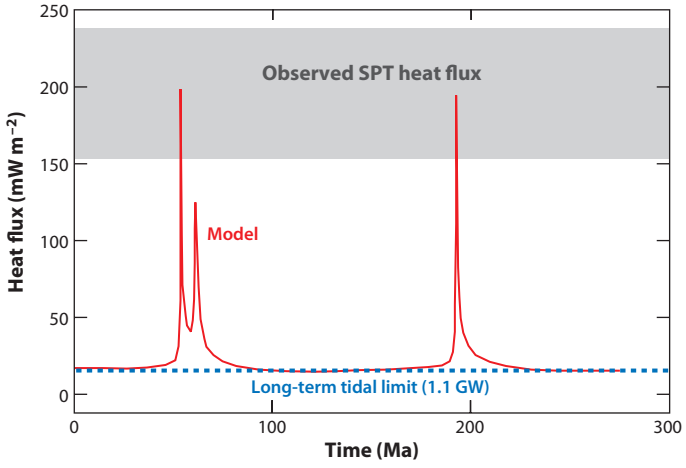

Figure 11

Numerical model results showing possible episodic heat release from Enceladus (modified from O'Neill & Nimmo 2010). The model is of two-dimensional Cartesian convection with yielding; high heat flux events occur when local yielding of the stagnant lid takes place. The long-term tidal heating of 1.1 GW is assumed to all be concentrated within the south polar terrain (SPT).

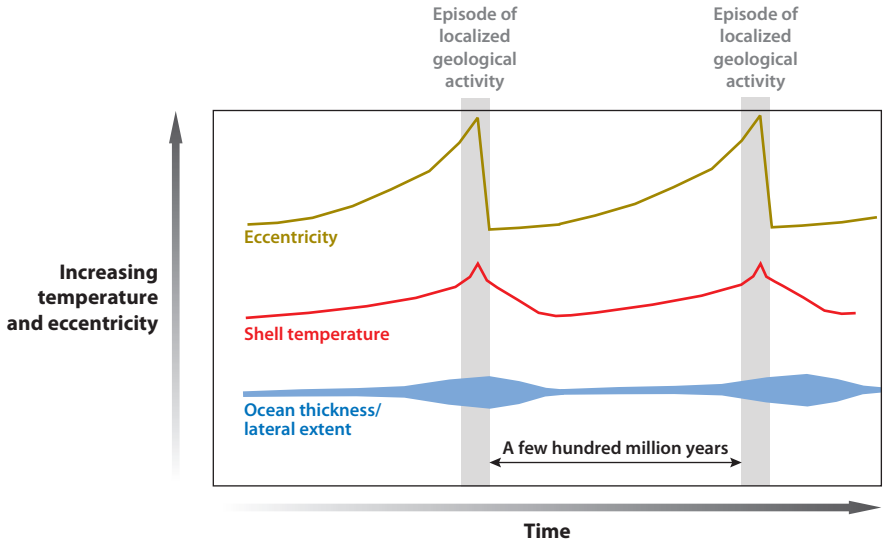

Figure 12

Diagram showing possible episodic heat generation in Enceladus. The satellite alternates between a relatively cold, nondissipative state in which the eccentricity increases and a warm, dissipative, tectonically active state in which the eccentricity is damped.

its time in a warm, dissipative state (as observed) in which eccentricity decreases and the rest of its time in a cold, nondissipative state in which eccentricity increases, thus satisfying the long-term heat production constraint of 1.1 GW (**Figure 12**). Such episodic heating can arise naturally—and potentially only within a restricted region—because of the strong feedback among heat production, temperature, and ice viscosity (e.g., Behounkova et al. 2012).

Fourth, the current heat flow may be overestimated, due for instance to the difficulty of modeling and removing the passive solar component from the observed thermal emission. If the heat flow is overestimated, the fraction of time that Enceladus can exhibit its current activity level increases, and the probability of seeing Enceladus in its current active state also increases. However, because much of the observed thermal emission is clearly associated with the tiger stripes (**Figure 7**) and thus must be endogenic, it is very unlikely that the reported 16-GW best-estimate power output (Howett et al. 2011) is overestimated by the factor of >14 that would be required for Enceladus to be currently in steady state.

Possibilities two and three suggest a duty cycle for Enceladus, in which it spends only ~10% of its time in an active state. Similarly, Enceladus currently has an apparent $k_2/Q = 0.01$ (Equation 1), but the time-averaged value of k_2/Q since its escape from an earlier resonance with Dione must be less than 0.0008 (Meyer & Wisdom 2008a, Zhang & Nimmo 2009). However, although episodic models currently seem attractive, their appeal must be balanced against the intrinsically low probability that we happen to be seeing Enceladus at an unusually active time.

3.5. Long-Term Geological and Ocean Evolution

The orbital arguments presented above suggest that Enceladus has spent most of its time in a cold, nondissipative state, interspersed with briefer (and perhaps spatially restricted) active episodes. The

geological evidence (Section 2.2) broadly supports this picture, suggesting that different regions of the body experienced periods of tectonic activity and high heat flux at different epochs.

A conductive or convective shell heated uniformly by 1.1 GW cannot sustain a global ocean over geological timescales (Roberts & Nimmo 2008a). However, 1.1 GW of heating focused around the south polar region can sustain a regional sea indefinitely (Behounkova et al. 2012, Tobie et al. 2008). Thus, Enceladus could well have maintained a regional ocean for as long as the current e-resonance with Dione has existed. Similar regional oceans in other locations at earlier times may explain the older activity that has affected the leading and trailing hemispheres of Enceladus.

3.6. Formation

The manner in which the satellites accreted from the protosatellite disk determines their initial thermal state and rock:ice ratio; both factors are of major importance in their subsequent evolution (e.g., Mosqueira et al. 2010). Unlike the Galilean satellites, the Saturnian satellites do not show a regular progression in ice:rock ratio with semimajor axis (e.g., Coradini et al. 2010). This is perhaps simply the result of incomplete radial mixing combined with the stochastic nature of the final stages of accretion. Late-stage impacts may have contributed to erosion of the icy mantle (Nimmo & Korycansky 2012) and perhaps even to the creation of ice-rich bodies (such as Tethys) as spallation products from a larger protosatellite (Sekine & Genda 2012).

Because of their small masses, neither Enceladus nor Mimas is likely to have been significantly heated by gravitational energy release during accretion. Thus, the main control on their initial thermal state—which in turn determined their propensity to undergo differentiation into a silicate interior and icy mantle—was the formation timescale compared with the decay timescale of ^{26}Al (0.7-Ma half-life) and the mass fraction of the silicates that host the ^{26}Al and other radiogenic heat sources. Satellite formation timescales in the inner disk are probably of order 0.1–1 Ma (Canup & Ward 2006, Mosqueira et al. 2010, Ogihara & Ida 2012), so it is certainly possible that Enceladus accreted while ^{26}Al was still active.

Mimas appears to have remained geologically inactive throughout its history (**Figure 2**) despite a current orbital eccentricity four times greater than that of Enceladus. Thus it is probably cold and rigid with a low k_2/Q and, hence, negligible tidal heating. The most likely explanation for the difference between Enceladus and Mimas is that, at some point, one or more resonances increased Enceladus's eccentricity enough to cause tidal heating sufficient to soften its interior. The softening process resulted in a runaway, because increasing temperatures lead to rigidity reduction and increased dissipation (e.g., Behounkova et al. 2012).

Alternatively, Mimas and Enceladus may have developed their differences when they formed (Schubert et al. 2007). Mimas has a smaller rock:ice ratio than does Enceladus and would, therefore, have experienced less heating by ^{26}Al. By contrast, because its semimajor axis is smaller than Enceladus's, Mimas probably accreted more rapidly, thus perhaps experiencing more ^{26}Al heating.

3.7. Summary

Most of the time and in most places, Enceladus's ice shell is probably cold, conductive, and not dissipative. Lateral density contrasts at relatively shallow depths are most likely responsible for the observed surface topography. The south polar topographic low, however, is caused by a regional subsurface sea, which is a geologically long-lived feature; localized convection is likely taking place in the ice shell above this sea. Enceladus probably exhibits brief bursts of localized activity and heat production interspersed with longer periods of dormancy. The difference between the geological histories of Enceladus and Mimas is most likely due to the different orbital histories of the two bodies.

4. UNDERSTANDING: SOUTH POLAR ACTIVITY

4.1. Tectonics

As described in Section 2.3, the SPT is a region of complex and currently poorly understood tectonic features. The marginal arcs and young north-trending fracture sets (**Figures 1** and ***6a***) probably indicate compression resulting from equatorward motion of material within the SPT. This lateral motion might arise from thermal expansion (Gioia et al. 2007), spreading away from the tiger stripes analogous to the terrestrial mid-ocean ridges (Helfenstein et al. 2008), or some other unknown cause may be responsible. Seafloor-like spreading—or some other kind of mobile-lid mechanism—is an attractive explanation for both the young age of the SPT and the high regional heat fluxes (Barr 2008). The unusual morphology of much of the terrain between the tiger stripes, reminiscent of pahoehoe lava flows (**Figure 6*c***), may be an indicator that mobile-lid convection is occurring, with a lid thickness of <400 meters (Barr & Preuss 2010).

Pathoff & Kattenhorn (2011) argue that the chaotic tectonic features within the SPT show a systematic progression in orientation with age. They also identified potential sets of ancient polar tiger stripes, although with different orientations to the current set, and concluded that nonsynchronous rotation had occurred. However, the limited number of clearly distinguishable cross-cutting relationships means these conclusions should be regarded as preliminary. Furthermore, significant nonsynchronous rotation is hard to reconcile with the symmetry of the global pattern of tectonic (and age) provinces about the current tidal axis.

It is not clear whether the topographic low associated with the SPT has played any role in surface tectonics. Subsidence of ∼0.5 km would generate polar compressional stresses of order 10 MPa (e.g., Janes & Melosh 1990), significantly larger than the diurnal tidal stresses of order 0.1 MPa (Nimmo et al. 2007). Reorientation and/or nonsynchronous rotation, if they occurred, would generate stresses of order 1 MPa (Matsuyama & Nimmo 2008). The reorientation scenario predicts east-west thrust faults in the south polar region, which may be present (Pathoff & Kattenhorn 2011), and east-west extensional stresses toward the equator, perhaps consistent with the observed young north-trending fracture sets. By contrast, the spatial distribution of impact craters does not support a recent episode of reorientation (Kirchoff & Schenk 2009). The present-day orientation of the tiger stripes maximizes the normal extensional tidal stresses (Nimmo et al. 2007), suggesting they began as tension cracks.

4.2. Plume Source and Mechanics

Evidence is accumulating that liquid water plays a role in the production of Enceladus's plumes. Initial arguments for a liquid-water source were based on the inference that the masses of gas and ice grains were comparable—a large ice grain mass could be a consequence of violent boiling of a liquid source directly into space (Porco et al. 2006). However, it is difficult to supply heat to a liquid exposed directly to space fast enough to prevent freezing (Postberg et al. 2009). In addition, subsequent observations that the grains are rich in sodium salts (Postberg et al. 2009, 2011) and the vapor is sodium poor (Schneider et al. 2009) imply that the two components are probably not generated by wholesale escape from the same source. However, the salty composition of the ice grains, which have a composition similar to that expected for water that has equilibrated with Enceladus's presumed silicate core (Zolotov 2007), currently provides strong evidence for a liquid-water source. It is very difficult to produce salty ice grains other than by flash freezing of salty liquid water—perhaps the most plausible alternative is that the plume is entraining salty grains that were formed in an earlier episode involving liquid water, but this is a more contrived

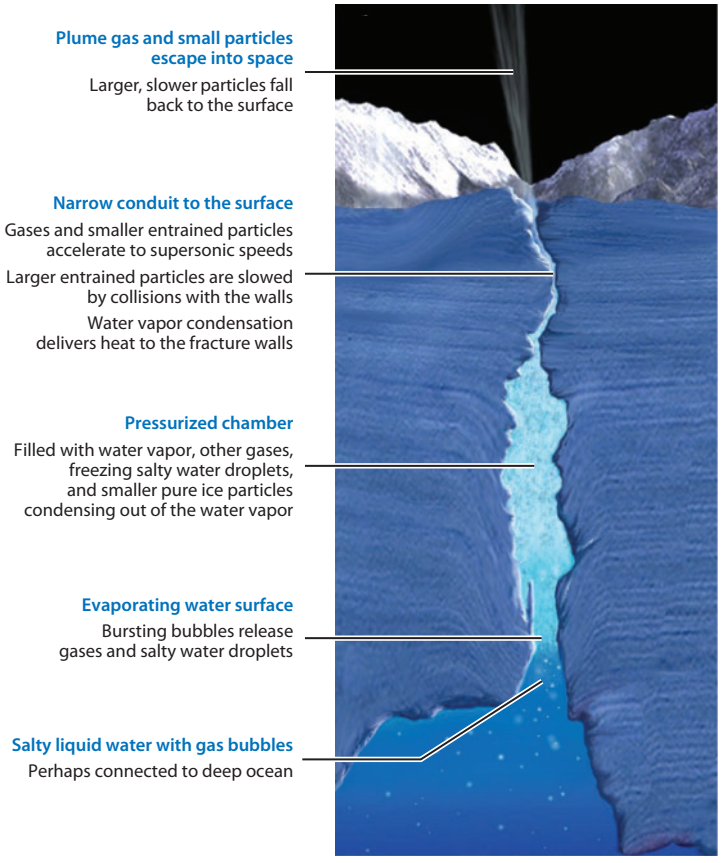

Figure 13

An artist's impression of the possible subsurface plumbing of a tiger stripe, showing the physical processes that may operate to generate the plume jets. Painting by Michael Carroll.

explanation. Postberg et al. (2009) avoid the problem of water freezing as it boils into a vacuum by proposing that the water evaporates more slowly, over a larger area, into pressurized chambers that then vent through narrow fractures to the surface (**Figure 13**). But a mechanism other than violent boiling is then needed to introduce the flash-frozen salty water droplets into the plume. Postberg et al. (2009) suggest the bursting of gas bubbles at the water surface as a possibility. The presence of gas bubbles in the water is plausible because the abundance of some plume gases, CO_2 and CH_4 in particular, is much higher than can be explained by their solubility in water (Waite et al. 2009). These gases must, thus, be introduced into the plume from a nonaqueous source, unless much of the water releases its dissolved gases and is then recycled back into the interior (Matson et al. 2012). Clathrate decomposition (Kieffer et al. 2006) has also been suggested as a possible source for the insoluble gases.

How heat is delivered to the plume source and to the surface where it is detected by Cassini is another question. The thermal signature is consistent with conductive heating of the surface by fractures with temperatures above 200 K (Abramov & Spencer 2009). The heat may be supplied by advection of plume gases up the fractures (Nimmo et al. 2007, Spencer et al. 2006) and then delivered to the near-surface ice by condensation of H_2O vapor on the fracture walls

(Ingersoll & Pankine 2010). Such condensation will close the cracks at a rate of up to ~1 m year^{-1}, potentially limiting the lifetime of individual active fractures. The heat might be generated at shallow depth by shear heating by diurnal tides (Nimmo et al. 2007), but the effectiveness of this mechanism depends on the efficiency of heat transport to the surface: Without efficient heat removal, the heating is self-limiting because increased temperature reduces the ice viscosity and, thus, the heating rate. Water ascending through cracks from the ocean can also bring heat to the surface (Matson et al. 2012, Porco et al. 2013) and gas bubbles in the water may reduce its density enough to allow it to rise buoyantly through the ice crust (Crawford & Stevenson 1988, Matson et al. 2012). Water pressure can help to keep fractures open (Crawford & Stevenson 1988). Changing diurnal tidal stresses may modulate plume activity (Hurford et al. 2007), and there is some observational evidence for such modulation (Gosmeyer et al. 2013). As they escape up the plume conduit into the vacuum of space, plume gases and particulates can be accelerated to the supersonic speeds that are inferred from the observations (Schmidt et al. 2008). Collisions with the conduit walls may explain the much slower speeds of many of the larger ejected particles.

5. IMPLICATIONS

5.1. Understanding Other Icy Satellites

Perhaps the most important lesson from Enceladus is that cryovolcanism—in the form of jetting activity—is a real phenomenon. It is interesting to speculate whether other tidally distorted bodies, such as Europa, also exhibit similar features: Europa has abundant double ridges that have morphological similarities to the tiger stripes, and shear-heating models developed to explain Europa's double ridges have been tested at Enceladus (Nimmo et al. 2007). However, so far, nothing strongly indicates that any of Europa's ridges are active. Europa possesses a tenuous asymmetric cloud of oxygen atoms that might be attributable to jet activity (Saur et al. 2011); the problem is that optical detection of Enceladus-like jets is made difficult by limited *Galileo* coverage and the likely reduced jet height due to Europa's higher gravity. Although Triton also has "geysers," these may be driven by near-surface, solar-powered processes (Kirk et al. 1990). Whether other kinds of cryovolcanism, such as proposed cryolava flows on Ganymede (Schenk et al. 2001), actually exist remains to be seen; there is no strong evidence for such flows on Enceladus.

A second lesson is that episodic activity, driven by orbital-thermal feedbacks, is not simply a theoretical argument but may actually occur. This conclusion adds weight to previous models suggesting that, for instance, Europa's young surface age is due to orbitally driven fluctuations in ice shell thickness (Hussmann & Spohn 2004). Satellites in this respect are quite different from the terrestrial planets, which are expected to experience more monotonic thermal histories; in this respect, they more closely resemble some exoplanets, many of which experience strong diurnal tides.

5.2. Habitability

In the case of Enceladus, the seemingly outrageous question of whether life exists there is well worth asking. The quest to understand how life came to exist on Earth and the search for other examples of life in the universe are driving goals for NASA's program of exploration. We do not yet understand the conditions required for the origin of life, but we do understand the conditions needed to sustain life similar to that on Earth. Three conditions must be met: a supply of the key elements used by life, liquid water, and a source of chemical energy. Of the elements essential to terrestrial life (carbon, hydrogen, nitrogen, oxygen, phosphorus, sulfur), all but phosphorous

(which is also likely to be present given its cosmochemical abundance) have been found in the Enceladus plume. There is also strong evidence for liquid water, as outlined above, and the plume has delivered samples from the potentially habitable zone to space, where they are available for analysis by spacecraft. Accordingly, Enceladus is one of the most exciting known targets for astrobiological study.

However, it is not clear whether Enceladus can satisfy the remaining requirement for habitability: a sufficient supply of chemical energy. Almost all life on Earth is ultimately powered by sunlight, which is not available in the subsurface environments where liquid water is likely on Enceladus (unless enterprising organisms have found a way to access the surface). However, a few known terrestrial microorganisms do not depend, directly or indirectly, on energy from sunlight, suggesting plausible mechanisms that may power Enceladan life (McKay et al. 2008). These mechanisms include generation of CH_4 from H_2 released by serpentinization of olivine (Stevens & McKinley 1995) and generation of H_2S from sulfates and hydrogen created by radioactive decay (Lin et al. 2006). Oxidants generated by radiolysis on Enceladus's surface and mixed into the interior by geological activity indicate another possible energy source (Parkinson et al. 2008). There is one important caveat, however: Episodic activity interspersed with long dormant periods may make Enceladus uninhabitable.

However, even if Enceladus proves to be uninhabited, or even uninhabitable, it can teach us much about the potential habitability of other icy worlds, because it is such a good place to study tidal heating. Tidal heating generates liquid-water environments that are independent of the heat from the host star, making it a powerful mechanism for expanding the habitable zone in this and probably other solar systems. Europa's subsurface ocean is another example in our own Solar System of a probable liquid-water environment, also potentially habitable, that is sustained by tidal heating. Similar examples are probably common in the Universe.

6. FUTURE EXPLORATION

Funding and spacecraft health permitting, the Cassini mission will continue through mid-2017, ending with destruction of the spacecraft in Saturn's atmosphere when its fuel is exhausted (Seal & Buffington 2009). Till then, Enceladus will continue to be a prime target, and the planned Cassini trajectory includes three more close flybys in 2015 as well as many distant observations of the plumes, surface, and south polar heat radiation. The decade-long record that Cassini will provide will begin to answer the question of the long-term stability of Enceladus's activity.

However, given the limitations of Cassini's orbit and instrumentation, there is much that it cannot tell us about Enceladus. For example, Cassini's infrequent and brief encounters with Enceladus do not allow it to map Enceladus's gravitational field or magnetic properties to probe its interior structure with the precision that could be achieved from Enceladus's orbit. Cassini cannot measure the tidal flexing of Enceladus to enable researchers to better understand its tidal heat engine. Cassini also cannot directly probe the plumbing of Enceladus's tiger stripes because it lacks a ground-penetrating radar. In addition, Cassini's ability to probe conditions at the plume source by measuring the composition and structure of the gas and particle plumes is limited by the mass range and resolution of its mass spectrometers. Because of the great discovery potential of future missions, Enceladus was named the equal-fourth highest priority target for future large planetary missions in the 2011 Planetary Decadal Survey, thus emphasizing its importance to planetary science and astrobiology (Space Stud. Board 2011). Although the Decadal Survey specifically recommended an Enceladus orbiter that would conduct detailed studies of plume composition and the geophysics of Enceladus, other mission architectures are plausible, including a plume sample return that would fly through the plume and return samples to Earth for analysis. While

we wait for future missions, ongoing study of the rich harvest of data from Cassini will continue to advance our understanding of this tiny but uniquely fascinating world.

DISCLOSURE STATEMENT

J.R.S. and F.N. both receive research funding from NASA. J.R.S. is a co-investigator, and F.N. is a participating scientist, on the NASA Cassini mission.

ACKNOWLEDGMENTS

We thank Robert Pappalardo for valuable comments on the manuscript and Jane Spencer for proofreading. We also thank everyone whose work on the Cassini mission has made possible the remarkable discoveries at Enceladus and throughout the Saturn system. J.R.S.'s work was supported in part by NASA grant NNX11AM47G.

LITERATURE CITED

Abramov O, Spencer JR. 2009. Endogenic heat from Enceladus' south polar fractures: new observations and models of conductive surface heating. *Icarus* 199:189–96

Barr AC. 2008. Mobile lid convection beneath Enceladus' south polar terrain. *J. Geophys. Res.* 113:E07009

Barr AC, McKinnon WB. 2007. Convection in Enceladus' ice shell: conditions for initiation. *Geophys. Res. Lett.* 34:L09202

Barr AC, Preuss LJ. 2010. On the origin of south polar folds on Enceladus. *Icarus* 208:499–503

Behounkova M, Tobie G, Choblet G, Cadek O. 2010. Coupling mantle convection and tidal dissipation: applications to Enceladus and Earth-like planets. *J. Geophys. Res.* 115:E09011

Behounkova M, Tobie G, Choblet G, Cadek O. 2012. Tidally-induced melting events as the origin of the south-pole activity on Enceladus. *Icarus* 219:655–64

Bland MT, Beyer RA, Showman AP. 2007. Unstable extension of Enceladus' lithosphere. *Icarus* 192:92–105

Bland MT, Singer KN, McKinnon WB, Schenk PM. 2012. Enceladus' extreme heat flux as revealed by its relaxed craters. *Geophys. Res. Lett.* 39:L17204

Brown RH, Clark RN, Buratti BJ, Cruikshank DP, Barnes JW, et al. 2006. Composition and physical properties of Enceladus' surface. *Science* 311:1425–28

Canup RM, Ward WR. 2006. A common mass scaling for satellite systems of gaseous planets. *Nature* 441:834–39

Cassidy TA, Johnson RE. 2010. Collisional spreading of Enceladus' neutral cloud. *Icarus* 209:696–703

Charnoz S, Crida A, Castillo-Rogez JC, Lainey V, Dones L, et al. 2011. Accretion of Saturn's mid-sized moons during the viscous spreading of young massive rings: solving the paradox of silicate-poor rings versus silicate-rich moons. *Icarus* 216:535–50

Chen EMA, Nimmo F. 2011. Obliquity tides do not significantly heat Enceladus. *Icarus* 214:779–81

Collins GC, Goodman JC. 2007. Enceladus' south polar sea. *Icarus* 189:72–82

Coradini A, Magni G, Turrini D. 2010. From gas to satellitesimals: disk formation and evolution. *Space Sci. Rev.* 153:411–29

Crawford, GD, Stevenson DJ. 1988. Gas-driven water volcanism in the resurfacing of Europa. *Icarus* 73:66–79

Crow-Willard E, Pappalardo RT. 2011. *Global geological mapping of Enceladus*. Presented at EPSC-DPS Jt. Meet., Oct. 2–7, Nantes, Fr. (Abstr. EPSC-DPS2011-635-1)

Dones L, Chapman CR, McKinnon WB, Melosh HJ, Kirchoff MR, et al. 2009. Icy satellites of Saturn: impact cratering and age determination. See Dougherty et al. 2009, pp. 613–35

Dougherty MK, Esposito LW, Krimigis SM, eds. 2009. *Saturn from Cassini-Huygens.* Dordrecht: Springer

Ducci M, Iess L, Armstrong JW, Asmar SW, Jacobson RA, et al. 2012. *The geodesy of the main Saturnian satellites from range rate measurements of the Cassini spacecraft*. Presented at Lunar Planet. Sci. Conf., 43rd, The Woodlands, Tex. (LPI Contrib. 1659, Abstr. 2200)

Emery JP, Burr DM, Cruikshank DP, Brown RH, Dalton JB. 2005. Near-infrared (0.8–4.0 mu m) spectroscopy of Mimas, Enceladus, Tethys, and Rhea. *Astron. Astrophys.* 435:353–62

Esposito LW, Colwell JE, Larsen K, McClintock WE, Stewart AI, et al. 2005. Ultraviolet imaging spectroscopy shows an active saturnian system. *Science* 307:1251–55

Giese B, Hussmann H, Roatsch T, Helfenstein P, Thomas PC, Neukum G. 2011. *Enceladus: evidence for librations forced by Dione*. Presented at EPSC-DPS Jt. Meet., Oct. 2–7, Nantes, Fr. (Abstr. 6:EPSC-DPS2011-976)

Giese B, Wagner R, Hussmann H, Neukum G, Perry J, et al. 2008. Enceladus: an estimate of heat flux and lithospheric thickness from flexurally supported topography. *Geophys. Res. Lett.* 35:L24204

Gioia G, Chakrobarty P, Marshak S, Kieffer SW. 2007. Unified model of tectonics and heat transport in a frigid Enceladus. *Proc. Natl. Acad. Sci. USA* 104:13578–81

Gosmeyer C, Hedman MM, Burns JA, Nicholson PD. 2013. *Variability in the particle plume of Saturn's moon Enceladus*. Presented at Am. Astron. Soc. Meet., 221st, Long Beach, Calif. (Abstr. 353.16)

Haff PK, Siscoe GL, Eviatar A. 1983. Ring and plasma: the enigmae of Enceladus. *Icarus* 56:426–38

Hamilton DP, Burns JA. 1994. Origin of Saturn's E ring: self-sustained, naturally. *Science* 264:550–53

Han L, Tobie G, Showman AP. 2012. The impact of a weak south pole on thermal convection in Enceladus' ice shell. *Icarus* 218:320–30

Hansen CJ, Shemansky DE, Esposito LW, Stewart AIF, Lewis BR, et al. 2011. The composition and structure of the Enceladus plume. *Geophys. Res. Lett.* 38:L11202

Hartogh P, Lellouch E, Moreno R, Bockelée-Morvan D, Biver N, et al. 2011. Direct detection of the Enceladus water torus with Herschel. *Astron. Astrophys.* 532:L2

Hedman MM, Nicholson PD, Showalter MR, Brown RH, Buratti BJ, Clark RN. 2009. Spectral observations of the Enceladus plume with Cassini-VIMS. *Astrophys. J.* 693:1749–62

Helfenstein P, Geise B, Ingersoll A, Johnson TV, McEwen AS, et al. 2008. *Enceladus south polar terrain geology: new details from Cassini ISS high resolution imaging*. Presented at AGU Fall Meet., San Francisco, Calif. (Abstr. P13D-02)

Hogenboom DL, Kargel JS, Consolmagno GJ, Holden TC, Lee L, Buyyounouski M. 1997. The ammonia-water system and the chemical differentiation of icy satellites. *Icarus* 128:171–80

Howett CJA, Spencer JR, Pearl J, Segura M. 2010. Thermal inertia and bolometric Bond albedo values for Mimas, Enceladus, Tethys, Dione, Rhea and Iapetus as derived from Cassini/CIRS measurements. *Icarus* 206:573–93

Howett CJA, Spencer JR, Pearl J, Segura M. 2011. High heat flow from Enceladus' south polar region measured using 10–600 cm^{-1} Cassini/CIRS data. *J. Geophys. Res.* 116:E03003

Hurford TA, Helfenstein P, Hoppa GV, Greenberg R, Bills BG. 2007. Eruptions arising from tidally controlled periodic openings of rifts on Enceladus. *Nature* 447:292–94

Hussmann H, Spohn T. 2004. Thermal-orbital evolution of Io and Europa. *Icarus* 171:391–410

Ingersoll AP, Ewald SP. 2011. Total particulate mass in Enceladus plumes and mass of Saturn's E ring inferred from Cassini ISS images. *Icarus* 216:492–506

Ingersoll AP, Pankine AA. 2010. Subsurface heat transfer to Enceladus: conditions under which melting occurs. *Icarus* 206:594–607

Janes DM, Melosh HJ. 1990. Tectonics of planetary loading: a general model and results. *J. Geophys. Res.* 95:21345–55

Jaumann R, Stephan K, Hansen GB, Clark RN, Buratti BJ, et al. 2008. Distribution of icy particles across Enceladus' surface as derived from Cassini-VIMS measurements. *Icarus* 193:407–19

Johnson RE, Smith HT, Tucker OJ, Liu M, Burger MH, et al. 2006. The Enceladus and OH tori at Saturn. *Astrophys. J.* 644:L137–39

Juhasz A, Horanyi M. 2002. Saturn's E ring: a dynamical approach. *J. Geophys. Res.* 107:1066

Kempf S, Beckmann U, Schmidt J. 2010. How the Enceladus dust plume feeds Saturn's E ring. *Icarus* 206:446–57

Kieffer SW, Lu X, Bethke CM, Spencer JR, Marshak S, Navrotsky A. 2006. A clathrate reservoir hypothesis for Enceladus' south polar plume. *Science* 314:1764–66

Kirchoff MR, Schenk P. 2009. Crater modification and geologic activity in Enceladus' heavily cratered plains: evidence from the impact crater distribution. *Icarus* 202:656–68

Kirk RL, Brown RH, Soderblom LA. 1990. Subsurface energy storage and transport for solar-powered geysers on Triton. *Science* 250:424–29
Lainey V, Karatekin Ö, Desmars J, Charnoz S, Arlot J-E, et al. 2012. Strong tidal dissipation in Saturn and constraints on Enceladus' thermal state from astrometry. *Astrophys. J.* 752:14
Lin L-H, Wang PL, Rumble D, Lippmann-Pipke J, Boice E, et al. 2006. Long-term sustainability of a high-energy, low-diversity crustal biome. *Science* 314:479–82
Matson DL, Castillo-Rogez JC, Davies AG, Johnson TV. 2012. Enceladus: a hypothesis for bringing both heat and chemicals to the surface. *Icarus* 221:53–62
Matsuyama I, Nimmo F. 2008. Tectonic patterns on reoriented and despun planetary bodies. *Icarus* 195:459–73
Mauk BH, Hamilton DC, Hill TW, Hospodarsky GB, Johnson RE, et al. 2009. Fundamental plasma processes in Saturn's magnetosphere. See Dougherty et al. 2009, pp. 281–331
McKay CP, Porco CC, Altheide T, Davis WL, Kral TA. 2008. The possible origin and persistence of life on Enceladus and detection of biomarkers in the plume. *Astrobiology* 8:909–19
McKinnon WB. 2011. *The shape of Enceladus' core: predictions for degree-2 nonhydrostatic gravity, and role in survival of the subsurface ocean*. Presented at EPSC-DPS Jt. Meet., Oct. 2–7, Nantes, Fr. (Abstr. 6:EPSC-DPS2011-1572-1)
Meyer J, Wisdom J. 2007. Tidal heating in Enceladus. *Icarus* 188:535–39
Meyer J, Wisdom J. 2008a. Tidal evolution of Mimas, Enceladus and Dione. *Icarus* 193:213–23
Meyer J, Wisdom J. 2008b. Episodic volcanism on Enceladus: application of the Ojakangas-Stevenson model. *Icarus* 198:178–80
Mitri G, Showman AP. 2008. A model for the temperature dependence of tidal dissipation in convective plumes on icy satellites: implications for Europa and Enceladus. *Icarus* 195:758–64
Morooka MW, Wahlund J-E, Eriksson AI, Farrell WM, Gurnett DA, et al. 2011. Dusty plasma in the vicinity of Enceladus. *J. Geophys. Res.* 116:A12221
Mosqueira I, Estrada P, Turrini D. 2010. Planetesimals and satellitesimals: formation of the satellite systems. *Space Sci. Rev.* 153:431–46
Murray CD, Dermott SF. 1999. *Solar System Dynamics*. Cambridge, UK: Cambridge Univ. Press. 608 pp.
Newman SF, Buratti BJ, Brown RH, Jaumann R, Bauer J, Momary T. 2008. Photometric and spectral analysis of the distribution of crystalline and amorphous ices on Enceladus as seen by Cassini. *Icarus* 193:397–406
Newman SF, Buratti BJ, Jaumann R, Bauer JM, Momary TW. 2007. Hydrogen peroxide on Enceladus. *Astrophys. J.* 670:L143–46
Nimmo F, Bills BG, Thomas PC. 2011. Geophysical implications of the long-wavelength topography of the Saturnian satellites. *J. Geophys. Res.* 116:E11001
Nimmo F, Korycansky DG. 2012. Impact-driven ice loss in outer Solar System satellites: consequences for the Late Heavy Bombardment. *Icarus* 219:508–10
Nimmo F, Pappalardo RT. 2006. Diapir-induced reorientation of Saturn's moon Enceladus. *Nature* 441:614–16
Nimmo F, Spencer JR, Pappalardo RT, Mullen ME. 2007. Shear heating as the origin of the plumes and heat flux on Enceladus. *Nature* 447:289–91
Ogihara M, Ida S. 2012. N-body simulations of satellite formation around giant planets: origin of orbital configuration of the Galilean moons. *Astrophys. J.* 753:60
Ojakangas GW, Stevenson DJ. 1986. Episodic volcanism of tidally heated satellites with application to Io. *Icarus* 66:341–58
O'Neill C, Nimmo F. 2010. The role of episodic overturn in generating the surface geology and heat flow on Enceladus. *Nat. Geosci.* 3:88–91
Parkinson CD, Liang MC, Yung YL, Kirschvink JL. 2008. Habitability of Enceladus: planetary conditions for life. *Orig. Life Evol. Biosph.* 38:355–69
Pathoff DA, Kattenhorn SA. 2011. A fracture history on Enceladus provides evidence for a global ocean. *Geophys. Res. Lett.* 38:L18201
Porco C, DiNino D, Nimmo F. 2013. *How the jets, heats and tidal stresses across the South Polar Terrain of Enceladus are related*. Presented at Lunar Planet. Sci. Conf., 44th, The Woodlands, Tex. (LPI Contrib. 1719)

Porco CC, Helfenstein P, Thomas PC, Ingersoll AP, Wisdom J, et al. 2006. Cassini observes the active south pole of Enceladus. *Science* 311:1393–401

Postberg F, Kempf S, Schmidt J, Brillantov N, Beinsen A, et al. 2009. Sodium salts in E-ring ice grains from an ocean below the surface of Enceladus. *Nature* 459:1098–101

Postberg F, Schmidt J, Hillier J, Kempf S, Srama R. 2011. A salt-water reservoir as the source of a compositionally stratified plume on Enceladus. *Nature* 474:620–22

Pryor WR, Rymer AM, Mitchell DG, Hill TW, Young DT, et al. 2011. The auroral footprint of Enceladus on Saturn. *Nature* 472:331–33

Roberts JH, Nimmo F. 2008a. Tidal heating and the long-term stability of a subsurface ocean on Enceladus. *Icarus* 194:675–89

Roberts JH, Nimmo F. 2008b. Near-surface heating on Enceladus and the south polar thermal anomaly. *Geophys. Res. Lett.* 35:L09201

Saur J, Feldman PD, Roth L, Nimmo F, Strobel DF, et al. 2011. Hubble Space Telescope advanced camera for surveys observations of Europa's atmospheric ultraviolet emission at eastern elongation. *Astrophys. J.* 738:153

Schenk P, Hamilton DP, Johnson RE, McKinnon WB, Paranicas C, et al. 2011. Plasma, plumes and rings: Saturn system dynamics as recorded in global color patterns on its midsize icy satellites. *Icarus* 211:740–57

Schenk PM, McKinnon WB. 2009. One-hundred-km-scale basins on Enceladus: evidence for an active ice shell. *Geophys. Res. Lett.* 36:L16202

Schenk PM, McKinnon WB, Gwynn D, Moore JM. 2001. Flooding of Ganymede's bright terrains by low-viscosity water-ice lavas. *Nature* 410:57–60

Schmidt J, Brilliantov N, Spahn F, Kempf S. 2008. Slow dust in Enceladus' plume from condensation and wall collisions in tiger stripe fractures. *Nature* 451:685–88

Schneider NM, Burger MH, Schaller EL, Brown ME, Johnson RE, et al. 2009. No sodium in the vapour plumes of Enceladus. *Nature* 459:1102–4

Schubert G, Anderson JD, Travis BJ, Palguta J. 2007. Enceladus: present internal structure and differentiation by early and long-term radiogenic heating. *Icarus* 188:345–55

Seal DA, Buffington BB. 2009. The Cassini extended mission. See Dougherty et al. 2009, pp. 725–44

Sekine Y, Genda H. 2012. Giant impacts in the Saturnian system: a possible origin of diversity in the inner mid-sized satellites. *Planet. Space Sci.* 63:133–38

Shemansky DE, Matheson P, Hall DT, Hu H-Y, Tripp TM. 1993. Detection of the hydroxyl radical in the Saturn magnetosphere. *Nature* 363:329–31

Smith BA, Soderblom L, Batson R, Bridges P, Inge J, et al. 1982. A new look at the Saturn system: the Voyager 2 images. *Science* 215:504–37

Sotin C, Head JW, Tobie G. 2002. Europa: tidal heating of upwelling thermal plumes and the origin of lenticulae and chaos melting. *Geophys. Res. Lett.* 29:1233

Space Stud. Board. 2011. *Visions and Voyages for Planetary Science in the Decade 2013–2022.* Washington, DC: Natl. Acad. Press. 400 pp.

Spencer JR, Barr AC, Esposito LW, Helfenstein P, Ingersoll AP, et al. 2009. Enceladus: an active cryovolcanic satellite. See Dougherty et al. 2009, pp. 683–724

Spencer JR, Howett CJA, Verbiscer AJ, Hurford TA, Segura ME, Pearl JC. 2011. *High-resolution observations of thermal emission from the south pole of Enceladus*. Presented at Lunar Planet. Sci. Conf., 42nd, The Woodlands, Tex. (LPI Contrib. 1608, Abstr. 2553)

Spencer JR, Pearl JC, Segura M, Flasar FM, Mamoutkine A, et al. 2006. Cassini encounters Enceladus: background and the discovery of a south polar hot spot. *Science* 311:1401–5

Spitale JN, Porco CC. 2007. Association of the jets of Enceladus with the warmest regions on its south polar fractures. *Nature* 449:695–97

Stevens TO, McKinley JP. 1995. Lithoautotrophic microbial ecosystems in deep basalt aquifers. *Science* 270:450–54

Stevenson DJ. 2000. *Limits on the variation of thickness of Europa's ice shell*. Presented at Lunar Planet. Sci. Conf., 31st, Houston, Tex. (Abstr. 1506)

Thomas PC. 2010. Sizes, shapes and derived properties of the Saturnian satellites after the Cassini nominal mission. *Icarus* 208:395–401

Tobie G, Cadek O, Sotin C. 2008. Solid tidal friction above a liquid water reservoir as the origin of the south pole hotspot on Enceladus. *Icarus* 196:642–52

Tyler R. 2011. Tidal dynamical considerations constrain the state of an ocean on Enceladus. *Icarus* 211:770–79

Verbiscer A, French R, Showalter M, Helfenstein P. 2007. Enceladus: cosmic graffiti artist caught in the act. *Science* 315:815

Waite JH, Lewis WS, Magee BA, Lunine JI, McKinnon WB, et al. 2009. Liquid water on Enceladus from observations of ammonia and ^{40}Ar in the plume. *Nature* 460:487–90

Waite JH, Magee B, Brockwell T, Zolotov MY, Teolis B, Lewis WS. 2011. *Enceladus plume composition*. Presented at EPSC-DPS Jt. Meet., Oct. 2–7, Nantes, Fr. (Abstr. 6:EPSC-DPS2011-61-4)

Wisdom J. 2004. Spin-orbit secondary resonance dynamics of Enceladus. *Astron. J.* 128:484–91

Zhang K, Nimmo F. 2009. Recent orbital evolution and the internal structures of Enceladus and Dione. *Icarus* 204:597–609

Zolotov MY. 2007. An oceanic composition on early and today's Enceladus. *Geophys. Res. Lett.* 34:L23203

Annual Review
of Earth and
Planetary Sciences
Volume 41, 2013

Contents